Hybrid Electromagnetic Modeling of Noise Interactions in Packaged Electronics Based on the Partial-Element Equivalent-Circuit Formulation

William Pinello, Andreas C. Cangellaris, *Member, IEEE*, and Albert Ruehli, *Fellow, IEEE*

***Abstract*— The partial-element equivalent-circuit (PEEC) method is used to develop a flexible, hierarchical electromagnetic modeling and simulation environment for the analysis of noise generation and signal degradation mechanisms in packaged electronic components and systems. The circuit-oriented approach used by the method for the development of the numerical approximation of the electric-field integral equation leads to SPICE-compatible, yet fully dynamic, discrete approximation of the electromagnetic problem. Contrary to other full-wave formulations, the proposed method has the important attribute of lending itself to a very systematic and physical model complexity reduction on the basis of the electrical size of the various portions of the system. Thus, a hybrid electromagnetic modeling and simulation environment is established for the analysis of complex structures which exhibit large variation in electrical size over their volume, using a combination of lumped-circuit elements, transmission lines, as well as three-dimensional (3-D) distributed electromagnetic models. These models may or may not account for retardation, depending on the electrical size of the part of the structure that is being modeled. These special attributes of the proposed electromagnetic-simulation environment are demonstrated through several examples from its application to the modeling of noise interactions in generic interconnect and package geometries.**

***Index Terms*—Circuit modeling, circuit transient analysis, integrated circuit interconnections, packaging, transient propagation, simulation.**

I. Introduction

TRANSIENT electromagnetic-field solvers have had a significant impact on our ability to model package- and interconnect-induced noise interactions in high-speed digital electronics systems. Unlike transmission-line-based simulation, the electromagnetic effects associated with the three-dimensional (3-D) character of the structures can be modeled accurately by such simulators. Consequently, in addition to crosstalk, propagation delay, and reflections, the impact of radiation losses due to unbalanced interconnects or other discontinuities in the interconnect and power/ground plane structures on signal distortion and internal and external electromagnetic compatibility of the component can be predicted and analyzed. Transient electromagnetic simulators in particular can be used for nonlinear electromagnetic analysis. Such simulation capability is important for accurate prediction of radiated emissions from high-speed digital electronic systems, and for electromagnetic noise analysis of mixed digital/analog/RF integrated circuits. Both the finite-difference time-domain (FDTD) method and the transmission line matrix (TLM) method have been used successfully for such nonlinear electromagnetic simulations [1]–[5].

Time-domain integral-equation-based formulations are also suitable for nonlinear electromagnetic analysis. However, the numerical instability exhibited by such formulations has prevented their extensive application to transient simulation of electromagnetic systems. The issue of numerical instability has been heavily researched over the last few years and the reasons for its occurrence are now fairly well understood. Several approaches have been proposed for its prevention [6]–[10].

Of particular interest to RF/microwave and high-frequency high-speed mixed-signal circuit electrical analysis is the partial-element equivalent-circuit (PEEC) formulation of the time-domain electric-field integral equation [11]. The reason for this is that this formulation results in a circuit model which includes all retardation effects and is compatible with nonlinear circuit simulators such as SPICE. Consequently, full-wave electromagnetic modeling within a SPICE-like nonlinear circuit simulation environment can be effected in a straightforward manner. Furthermore, once the PEEC model for an electromagnetic system has been developed, a systematic procedure can be used to reduce its complexity, taking into account the characteristic times over which the system response is sought, or, equivalently, the electrical size of the structure under study. For example, if the characteristic time of the excitation (i.e., the rise time of a pulsed excitation or the period of a time-harmonic excitation) is such that useful wavelengths are much larger than the spatial extent of the system, all retardation effects can be neglected. Moreover, such model complexity reduction can be effected in a selective fashion over those parts of the structure where the aforementioned electrical size constraints are valid. This attribute of the PEEC formulation is extremely useful when

Manuscript received January 31, 1997; revised May 23, 1997.

W. Pinello is with the Center for Electronic Packaging Research, Electrical and Computer Engineering Department, University of Arizona, Tucson, AZ 85721 USA.

A. C. Cangellaris was with the Department of Electrical and Computer Engineering, University of Arizona, Tucson, AZ 85721 USA. He is now with the Department of Electrical and Computer Engineering, University of Illinois at Urbana–Champaign, Urbana, IL 61801 USA.

A. Ruehli is with I. B. M. Research Division, T. J. Watson Research Center, Yorktown Heights, NY 10598 USA.

Publisher Item Identifier S 0018-9480(97)07388-2.

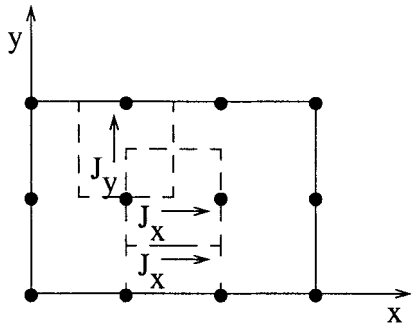

Fig. 1. 2-D discretization of current density.

the size or complexity of the structure is such that the number of degrees of freedom used in the numerical approximation is much larger than the one required for acceptable engineering accuracy of the simulation results. Clearly, this is the case for packaged electronics. These systems are very representative cases of multiscale electromagnetic structures in the sense that they exhibit large variability in the electrical size of their various components and subsystems.

It is the purpose of this paper to demonstrate the impact of the aforementioned attributes of the PEEC method to the electromagnetic modeling of interconnect and packaging structures often encountered in computing and communication subsystems and modules. First, a brief review of the development of the PEEC models is presented, along with the circuit analysis-compatible formulation of the discrete approximation of the resulting distributed network. This is followed by the discussion of the process through which model complexity reduction is effected. Numerical examples are presented that help validate the method and illustrate its application to the electromagnetic analysis of several generic packaging structures.

II. Development of PEEC Models

As discussed in detail in [11], the development of the PEEC approximation of an electromagnetic boundary value problem is based on the proper electromagnetic interpretation of the various terms in the equation

$$-\frac{\partial}{\partial t}\overline{A}(\overline{r},t)-\nabla\Phi(\overline{r},t)=\overline{E}(\overline{r},t) \tag{1}$$

where $\overline{A}$ and Φ are the vector magnetic and scalar electric potentials, respectively, and $\overline{E}$ is the electric-field vector at some point in space and time. The potentials are defined in a K conductor system by

$$\overline{A}(\overline{r},t)=\sum_{k=1}^{K}\frac{\mu}{4\pi}\int_{v_k}\frac{\overline{J}(\overline{r}',t')}{|\overline{r}-\overline{r}'|}\,dv' \tag{2}$$

and

$$\Phi(\overline{r},t)=\sum_{k=1}^{K}\frac{1}{4\pi\varepsilon}\int_{v_k}\frac{q(\overline{r}',t')}{|\overline{r}-\overline{r}'|}\,dv' \tag{3}$$

where $t'=t-|\overline{r}-\overline{r}'|/v$ denotes the retardation time in a medium with propagation speed v. $\overline{J}$ is the current density, and q is the charge density. To keep the presentation simple, the media surrounding the conductors are assumed to be homogeneous with permeability μ and permittivity ε. The generalization of the model for the case of inhomogeneous dielectrics is possible and is effected through the use of polarization currents [12]. This way, for the case of conductors of finite extent, homogeneous-medium Green's functions are used in the integral representations of the potentials, as shown in the equations above. With these assumptions, inserting (2) and (3) into (1), and enforcing (1) at a point inside one of the conductors, we obtain an expression involving the unknown quantities $\overline{J}$ and q as follows:

$$\frac{\overline{J}(\overline{r},t)}{\sigma}+\frac{\partial}{\partial t}\sum_{k=1}^{K}\frac{\mu}{4\pi}\int_{v_k}\frac{\overline{J}(\overline{r}',t')}{|\overline{r}-\overline{r}'|}\,dv' +\sum_{k=1}^{K}\frac{1}{4\pi\varepsilon}\nabla\left[\int_{v_k}\frac{q(\overline{r}',t')}{|\overline{r}-\overline{r}'|}\,dv'\right]=0 \tag{4}$$

where σ is the conductivity at the specific point inside the conductor. In order to solve the system of equations in (4), the current and charge densities are discretized into volume and surface cells, respectively. The volume cells give a 3-D representation of the current flow through a finite cross section, while the surface cells effect a two-dimensional (2-D) representation of the charge over the surface of the corresponding volume cell. This discretization is achieved mathematically by defining the rectangular pulse functions

$$P_{\gamma nk}=\begin{cases}1, & \text{inside the } nk\text{th volume cell}\\ 0, & \text{elsewhere}\end{cases} \tag{5}$$

for the current density where $\gamma=x,y,z$ indicates the component of the current in the nth volume cell of the kth conductor and

$$p_{mk}=\begin{cases}1, & \text{on the } mk\text{th surface cell}\\ 0, & \text{elsewhere}\end{cases} \tag{6}$$

for the charge density on the mth surface cell of the kth conductor. Fig. 1 shows in top view the manner in which a conductor is segmented into volume cells. The level of discretization, i.e., the dimensionality of the current flow, is determined by the shape of the conductor, the shape of the surrounding conductors, and the frequency range of interest. In most applications it is acceptable to use one-dimensional (1-D) or 2-D current distrubution. However, if the impact of skin-effect on the response is desired, a full 3-D distrubution is required. For simplicity, all of the examples in this paper use 1-D and 2-D currents. Fig. 2 shows the discretization of the charge density on one of the surface cells. For this case, if the conductor is not infinitesimally thin, the conductor must also be discretized on the remaining five surfaces. In addition, if 3-D current flow is not taken into account for

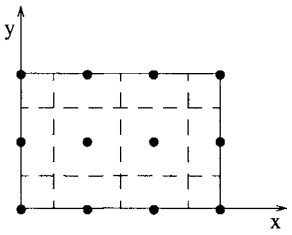

Fig. 2. 2-D discretization of charge density.

this truly 3-D conductor, then the unknown charges which are associated with at the nodes shown by the dots in Fig. 2, must be connected between the top- and bottom-surface cells of a volume cell. This is an acceptable approximation when the current distribution along the thickness of the conductor can be assumed uniform.

Given the definition of the pulse functions in (5) and (6), the current and charge densities are approximated over each of the k conductors by

$$J_{\gamma k}(\overline{r}, t') = \sum_{n=1}^{N_{\gamma k}} P_{\gamma nk} J_{\gamma nk}(t_n) \tag{7}$$

and

$$q_k(\overline{r}, t') = \sum_{m=1}^{M_k} p_{mk} q_{mk}(t_m) \tag{8}$$

where $t_n = t - |\overline{r} - \overline{r}'_n|/v$, $t_m = t - |\overline{r} - \overline{r}'_m|/v$, $\overline{r}'_n$ is the position vector of the of the n th volume cell and $\overline{r}'_m$ is the position vector of the center of the equipotential surface associated with the mth surface cell. Additionally, $N_{\gamma k}$ denotes the number of volume cells for conductor k with γ-directed current and M_k denotes the number of surface cells for conductor k.

Substituting (7) into (4), we get for a point inside the mth cell of the lth conductor

$$\frac{J_{\gamma ml}(t)}{\sigma} + \frac{\partial}{\partial t} \sum_{k=1}^{K} \sum_{n=1}^{N_{\gamma k}} \frac{\mu}{4\pi} \left[\int_{v_k} \frac{P_{\gamma nk} J_{\gamma nk}(t_n)}{|\overline{r} - \overline{r}'|} \, dv' \right] + \sum_{k=1}^{K} \frac{\partial}{\partial \gamma} \left[\frac{1}{4\pi\varepsilon} \int_{v_k} \frac{q(\overline{r}', t')}{|\overline{r} - \overline{r}'|} \, dv' \right] = 0. \tag{9}$$

This step is followed by the testing of the resulting equation in the Galerkin approximation sense (i.e., the aforementioned pulse functions used for the expansion of the current and charge densities are also used for testing) utilizing an inner product over the volume of a cell defined as follows:

$$\frac{1}{a_m} \int_{v_m} f(\overline{r}) dv = \frac{1}{a_m} \int_{a_m} \int_{l_m} f(\overline{r}) da dl \tag{10}$$

where v_m is the volume of cell m, a_m is the cross section of the cell, l_m is its length, and $f(\overline{r})$ is the integrand. This process leads to a system of equations of the form

$$\frac{I_{\gamma ml}(t) l_m}{a_{\gamma ml} \sigma} + \sum_{k=1}^{K} \sum_{n=1}^{N_{\gamma k}} \frac{\mu}{4\pi} \frac{1}{a_{\gamma ml}} \frac{1}{a_{\gamma nk}} \cdot \int_{v_{ml}} \int_{v_{nk}} \frac{\frac{\partial}{\partial t} I_{\gamma nk}(t_n)}{|\overline{r} - \overline{r}'|} dv' dv_{ml} + \sum_{k=1}^{K} \frac{1}{4\pi\varepsilon} \int_{v_{ml}} \frac{\partial}{\partial \gamma} \int_{S_k} \frac{q(\overline{r'}, t')}{|\overline{r} - \overline{r}'|} ds' dv_{ml} = 0 \tag{11}$$

where we make the identification that $J_\gamma(t) = I_\gamma(t)/a$ and convert the volume integration to a surface integration for the third term since the charge only resides on the surface of the volume. Next, the approximation

$$\int_{v_l} \frac{\partial}{\partial \gamma} F(\gamma) dv_l \approx a_l \left[F\left(\gamma + \frac{l_m}{2}\right) - F\left(\gamma - \frac{l_m}{2}\right) \right] \tag{12}$$

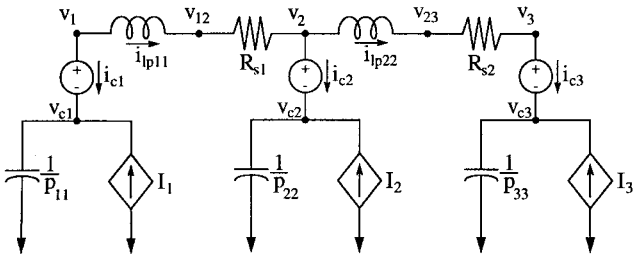

Fig. 3. Two-cell PEEC model with series resistances.

is used with (8) to further reduce (11) to

$$\frac{I_{\gamma ml}(t) l_m}{a_{\gamma ml} \sigma} + \sum_{k=1}^{K} \sum_{n=1}^{N_{\gamma k}} \frac{\mu}{4\pi} \frac{1}{a_{\gamma ml}} \frac{1}{a_{\gamma nk}} \cdot \int_{v_{ml}} \int_{v_{nk}} \frac{\frac{\partial}{\partial t} I_{\gamma nk}(t_n)}{|\overline{r} - \overline{r}'|} dv' dv_{ml} + \sum_{k=1}^{K} \sum_{m=1}^{M_k} \left[q_{mk}(t_m) \frac{1}{4\pi\varepsilon} \int_{S_{mk}} \frac{1}{|\overline{r}^+ - \overline{r}'|} ds' - q_{mk}(t_m) \frac{1}{4\pi\varepsilon} \int_{S_{mk}} \frac{1}{|\overline{r}^- - \overline{r}'|} ds' \right] = 0. \tag{13}$$

This is the desired form of the discrete approximation of the electric-field integral equation, from which the various types of the equivalent circuits can be inferred. The development of the overall PEEC circuit is effected by combining the equations in (13) for the voltage drop along each appropriate direction in a conductor cell with the discrete version of the conservation of charge equation. More specifically, the discrete implementation of the conservation of charge equation is effected through the enforcement of Kirchoff's current law in the resulting PEEC circuit.

Fig. 3 depicts the PEEC circuit for two adjacent conducting cells of zero thickness. The self resistances R_{si} are easily associated with the first term in (13), while the partial inductances L_{pij} and coefficients of potential p_{ij} are obtained from the calculation of the integrals in the second and third terms in (13), respectively. It is important to recognize that retardation is taken into account in the coupling between the lumped inductors and capacitors, a fact that is evident from the presence of the retarded times in the time-dependence of the currents through the inductors and the charges at the capacitors. Thus, despite the deceiving equivalent circuit representation of the discrete form of the boundary-value problem, the full-wave electromagnetic nature of the problem is preserved. From Fig. 3, the compatibility of the PEEC model with standard lumped-circuit simulation practices becomes apparent. In particular, the use of the modified nodal analysis (MNA) matrix formulation for the state representation of the PEEC model makes it directly compatible with SPICE-like circuit simulators, where the unknowns used are nodal voltages, which for the electromagnetic case corresponds to the potentials with respect to infinity, and the inductance branch currents. The source terms are in the form of current and voltage sources that include both point excitation and distributed excitation (e.g., incident electromagnetic fields).

For the PEEC model shown in Fig. 3, the corresponding MNA equations are shown in (14) at the bottom of the page, where

$$\alpha = -\frac{p_{12}}{p_{11}}(\tau_{p12}) \tag{15}$$

$$\beta = \frac{p_{12}}{p_{11}}(\tau_{p12}) - \frac{p_{13}}{p_{11}}(\tau_{p13}) \tag{16}$$

$$\gamma = \frac{p_{12}}{p_{22}}(\tau_{p12}) \tag{17}$$

$$\varepsilon = \frac{p_{13}}{p_{33}}(\tau_{p13}) - \frac{p_{23}}{p_{33}}(\tau_{p23}) \tag{18}$$

$$\phi = \frac{p_{23}}{p_{33}}(\tau_{p23}). \tag{19}$$

$G_{ii} = 1/R_{ii}$, the argument τ_{pij} is the center-to-center delay from node i to node j, indicating a delayed interaction between the two nodes, and the argument τ_{Lij} is the center-to-center delay from cell i to cell j. The value of I_i at each of the current-controlled current sources is given by

$$I_{i(t)} = \sum_{\substack{j=1 \\ i \neq j}}^{3} \frac{p_{ij}}{p_{ii}} I_j(t - \tau_{pij}) \tag{20}$$

and the value of the branch voltage across each inductor is

$$V_{L_{ii(t)}} = \sum_{j=1}^{2} Lp_{ij} \frac{\partial}{\partial t} I_j(t - \tau_{Lij}). \tag{21}$$

III. Hierarchical Electromagnetic Modeling of Interconnect Networks

As already mentioned, the two key attributes of the PEEC formulation are its ability to model *heterogeneous* systems (i.e., systems involving lumped-circuit elements as well as distributed electromagnetic components) and its suitability for hierarchical electromagnetic modeling. This second attribute is closely related to model complexity (or model order) reduction, and it is of critical importance to the efficiency with which electromagnetic analysis of interconnect and packaging structures associated with high-speed digital and high-frequency analog electronics can be effected.

A review of the applications of PEEC to electromagnetic simulation reveals that the most popular model-complexity reduction has been the elimination of the delays in PEEC models. Clearly, this approximation is acceptable when the size of the structures under investigation is small compared to the minimum wavelength of interest. As an example, we mention the application of PEEC for the electrical modeling of single-chip package interconnects in terms of a network of resistors, partial inductances, and potential coefficients. Furthermore, if only the inductive behavior of the package is of interest, the PEEC model reduces to the so-called (L_p, R) PEEC model, which is essentially a discrete approximation of the magnetic diffusion equation, and has been used extensively for package inductance modeling [13], [14].

The implementation of the PEEC formulation in a SPICE-compatible simulator provides for a more versatile application of the aforementioned quasi-static reduced PEEC models. More specifically, different levels of interconnect and different parts in the package and board of a system can be modeled for the purpose of signal integrity prediction by implementating different types of electrical models as appropriate. For example, an (L_p, P, R) PEEC model can still be used to model the interconnects and associated ground and power planes within a single-chip package, with SPICE models for the driver electronics and SPICE-compatible transmission-line models for the coupled interconnects on the integrating substrate card or board. This way, very complex interconnect/packaging structures can be modeled efficiently using a single modeling/simulation environment.

In the aforementioned example, it is assumed that the emphasis of the simulation is on the prediction of signal degradation due to crosstalk, interconnect delay, reflection, and simultaneous switching noise. If, in addition, the prediction of electromagnetic radiation from the interconnect and package structure is of interest, the aforementioned model becomes inadequate, and retardation effects need be taken into account. Furthermore, if it is possible to identify the dominant sources of radiation, the delays can be incorporated selectively and in a limited fashion where appropriate. For example, selected interconnects on printed circuit boards, which exhibit imbalances due to discontinuities or layout constraints, can be modeled using a rigorous electromagnetic PEEC model, while the remaining well-balanced interconnects can be modeled using SPICE-compatible transmission-line models.

Finally, it is mentioned that this hierarchical capability of the proposed simulator is very suitable for efficient electromagnetic analysis of mixed-signal electronics, where interactions between the interconnect and power/ground distribution networks for the high-speed digital and the analog/RF blocks need to be taken into account for proper electrical design. As an example, we mention the case where noise generated in the digital block of a portable computing device is radiated out and eventually received by an antenna used for providing a wireless data link for the device. A generic example of such an interaction is presented Section IV.

$$\begin{bmatrix} \frac{1}{p_{11}}\frac{\partial}{\partial t} & G_{11} & -G_{11} & 0 & 0 & 1+\alpha & \beta \\ 0 & -G_{11} & G_{11} & 0 & 0 & -1+\gamma & \delta \\ 0 & 0 & \frac{1}{p_{22}}\frac{\partial}{\partial t} & 0 & G_{22} & -G_{22}+\varepsilon & 1+\phi \\ 0 & 0 & 0 & 0 & -G_{22} & G_{22} & -1 \\ 0 & 0 & 0 & 0 & \frac{1}{p_{33}}\frac{\partial}{\partial t} & 0 & 0 \\ 1 & -1 & 0 & 0 & 0 & -L_{p11}\frac{\partial}{\partial t} & -L_{p12}\frac{\partial}{\partial t}(\tau_{L12}) \\ 0 & 0 & 1 & -1 & 0 & -L_{p12}\frac{\partial}{\partial t}(\tau_{L12}) & -L_{p22}\frac{\partial}{\partial t} \end{bmatrix} \begin{bmatrix} v_1 \\ v_{12} \\ v_2 \\ v_{23} \\ v_3 \\ i_{lp11} \\ i_{lp22} \end{bmatrix} = \begin{bmatrix} 0 \\ 0 \\ 0 \\ 0 \\ 0 \\ 0 \\ 0 \end{bmatrix} \tag{14}$$

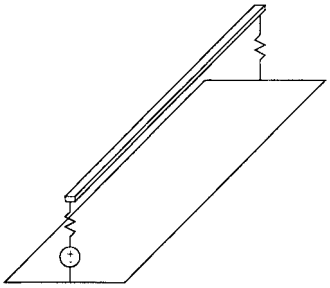

Fig. 4. Interconnect above a solid ground plane.

IV. Numerical Results

For a hierarchical electromagnetic analysis of interconnect and packaging structures in the sense described in Section III, a special-purpose PEEC simulator has been developed which is capable of handling linear elements. This simulator includes parameter extraction modules for the calculation of equivalent partial inductances and potential coefficients of the geometry under study as well as a new version of a circuit simulator, which mimics SPICE [15], with all the necessary enhancements to accommodate electromagnetic retardation. The following numerical examples illustrate some of the capabilities of the simulator.

In order to effect an accurate and efficient solution for a system constructed from the PEEC formulation, it is necessary to discretize the conductors in such a way as to limit the number of unknowns without compromising the accuracy of the solution. As a first step, conductors representing pin's, vias, and traces are usually discretized along their length with 20 elements per wavelength corresponding to the highest frequency of interest. Ground and power planes are discretized in a similar fashion, except that 2-D current flow is accounted for. In all cases, for simplicity, effects from skin-effect are neglected. Once the geometry is discretized, then the corresponding partial inductances and potential coefficients are calculated according to the PEEC formulation, thus resulting in an equivalent circuit model consistent with Maxwell's equations.

After the equivalent-circuit elements are computed, the system is solved in the time or frequency domain using modified nodal analysis. For the time-domain solution where retardation is present, late time instability is still a concern and ultimately dictates the minimum time-step allowed. Recent progress in this area has led to better understanding of the sources of instability, as well as new methodologies for its suppression. The effectiveness of these new approaches is currently under further investigation. For the simulator used to obtain results for this paper, the procedure for the selection of the optimum time-step was an *ad-hoc* one and was based on convergence studies for the specific problem at hand. The issue of convergence is related to the fact that the numerical integration used for this study—Backward–Euler—is dissipative, a property which enhances numerical stability but may result in unacceptable artificial damping of the solution. Thus, it is important to choose the time-step carefully so that enhanced stability is achieved without unacceptable numerical damping. Since numerical damping is controlled by using small time-steps, the *ad-hoc* procedure for the selection of the time-step is as follows. The initial value for the time-step is taken to be in the order of 10% of the rise time of the excitation pulse. Then it is decreased until convergence is reached or the solution becomes unstable. The following numerical examples illustrate some of the capabilities of this approach for obtaining PEEC solutions.

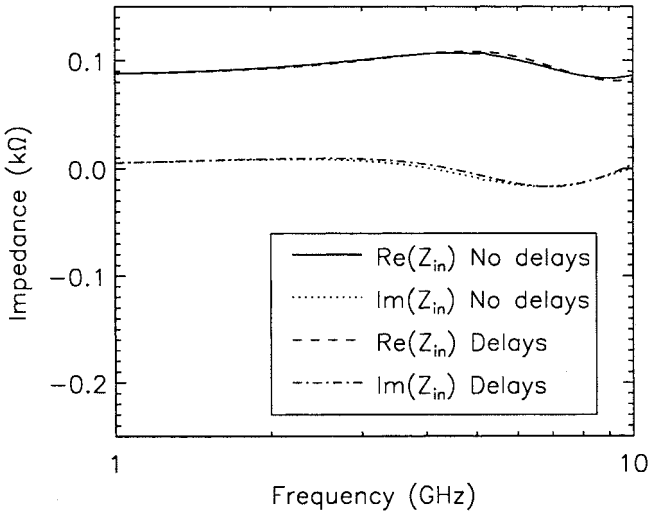

Fig. 5. Input impedance for active line above a solid ground plane.

The first example for the geometry shown in Fig. 4 consists of an interconnect above a finite ground plane and is used for code validation purposes. The line is driven by a voltage source and terminated by 86-Ω resistors at each end. The ground plane is 2.0 cm long by 1.0 cm wide and divided into 20 cells along the length and six cells along the width. The line, placed 0.5 mm above the ground plane, is 2.0 cm long with a width of 1 mm. It is divided into 20 cells along the length. For this example, 2-D current flow is only accounted for on the ground plane.

Since the layout of the conductors in this example models quite closely the effects of a simple two-conductor transmission line, the current distribution along the line and the return ground path are expected to exhibit the differential mode character of transmission-line currents. As a result, the solution from a full-wave electromagnetic analysis should be almost identical with the one predicted using a method of characteristics model with the appropriate transmission-line impedance and delay. The PEEC model without retardation is somewhat like the method of characteristics model, except that the longitudinal couplings are also included. Fig. 5 depicts the variation of the input impedance of the line versus frequency calculated using the PEEC formulation with and without delays.

Alternatively, if the arrangement of conductors results in a response which cannot be accurately described by the method of characteristics models due to the presence of discontinuities and other interconnect features that give rise to electromagnetic radiation, then it is imperative to include the retardation in the simulation. The geometry shown in Fig. 6 depicts an interconnect crossing a gap between two conducting plates. These types of structures occur frequently in packages for mixed-signal electronics where separate ground planes are used for the digital and analog blocks. The presence of the slot in the ground plane results in slot-line modes which

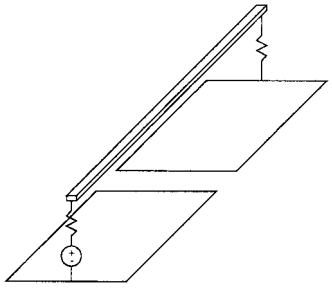

Fig. 6. Interconnect above a split ground plane.

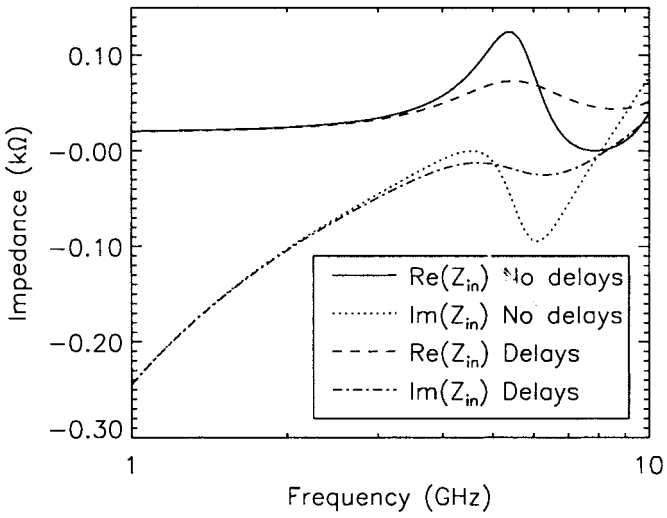

Fig. 7. Input impedance for active line above a split ground plane.

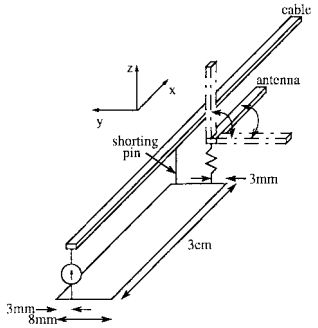

Fig. 8. Geometry for the second example.

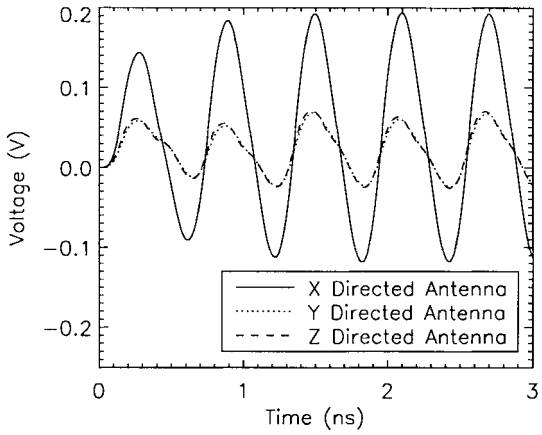

Fig. 9. Voltage across the load resistor of the antenna in Fig. 8 calculated without the shorting pin.

eventually lead to energy loss through radiation. To illustrate this phenomenon, the structure of Fig. 6 was simulated. The dimensions and discretization for this geometry are the same as the previous example, except that the ground plane is now split into two equal halves with 1-mm separation. Fig. 7 shows the input impedance of the line for this case. It is clear that the calculated impedances with and without retardation are very different for the higher frequencies where the resonant properties of the structure and radiation effects dominate the response. This is due to the fact that the energy which is radiated from the slot can only be accounted for accurately when retardation effects are included.

The second example deals with the modeling of electromagnetic radiation caused by the presence of parasitic high-frequency current flowing in the attached cables of printed circuit boards [16]. This source of noise is modeled with a generic structure as shown in Fig. 8. The high-frequency digital noise flowing through the cable is modeled by a current source which generates a periodic sequence of trapezoidal shaped pulses. The rise, roof, and fall times are 0.1 ns and the period of the signal is 0.6 ns. The current amplitude is 10 mA. The length of the cable is 15 cm. It is modeled as an infinitesimally thin strip of width 1.0 mm. The cable runs parallel to a finite ground plate of width 0.8 cm and length of 3.0 cm. It is positioned 0.5 mm above the plate. The receiving element for the radiation caused by the protruding cable is a wire monopole connected at the other end of the ground plate with a terminating resistance of 35 Ω. The antenna length is 8.0 cm and it is modeled as an infinitesimally thin strip of width 1.0 mm. Three possible arrangements of the antenna will be compared, as shown in Fig. 8. The PEEC model for this structure is developed assuming 1-D current for the wires and 2-D current for the ground plate. Fig. 9 shows the voltage across the load resistor for the three arrangements of the receiving antenna in the absence of the shorting pin. As expected, the coupled noise voltage exhibits a time-harmonic variation of frequency consistent with the effective length of the structure formed by the antenna and the ground plate. In particular, the frequency of the time-harmonic variation of the voltage for the x-directed antenna is approximately 1.67 GHz which corresponds to a wavelength of 18.0 cm. The combined length of the antenna with the ground plate is 8.0 cm which is approximately half-wavelength at the aforementioned frequency. The visualization of the current flow along the wires and the magnitude of the current density at $f = 1.67$ GHz is shown in Fig. 10.

Fig. 11 shows the voltage across the load resistor of the receiving antenna when a pin is used to short the cable to the ground plate, as shown in Fig. 8. Since the presence of the pin allows for a very low impedance path for the noise current back to its source, the radiated emissions are minimized. In practice, this noise suppression is often effected using ferrite beads.

The last example deals with an interconnect configuration that is often encountered in single-chip packages without a ground plane. In such packages, ground is brought to the die through conducting traces in the package. These ground

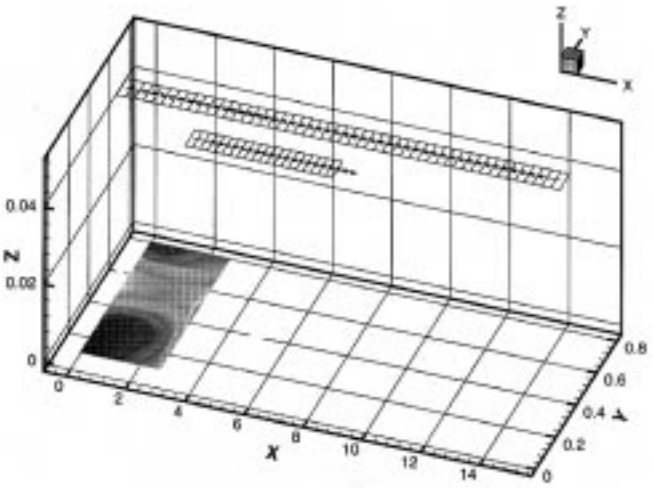

Fig. 10. Current distribution on the conductors of the structure in Fig. 8 at $f = 1.67$ GHz.

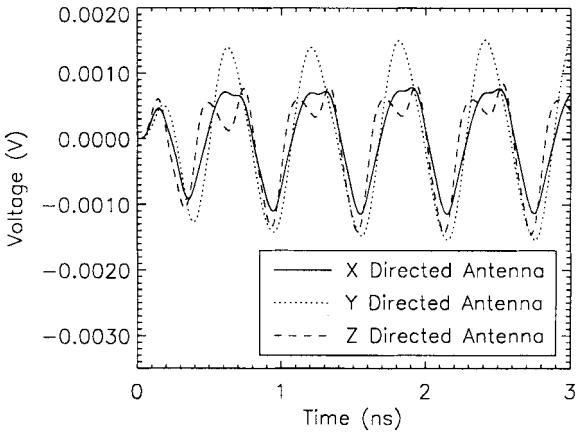

Fig. 11. Voltage across the load resistor of the antenna in Fig. 8 calculated with the shorting pin.

traces are then connected to a ground ring or some other ground pad at the periphery of the package. These types of connections result in unbalanced interconnects which, as is well known, give rise to radiation. Even though this radiation is part of the overall electromagnetic behavior of the resulting interconnect structure, it is customary to quantify the amount of this radiation in terms of the so-called common-mode component in the current flowing through the interconnect [17]. Figs. 12 and 13 depict two cases of such interconnects. In Case 1, the ground trace is connected to the ground pad at a distance of 2.5 cm from the signal trace, while in Case 2 the ground pin is placed right next to the signal trace. In both cases, the traces are 1 mm wide with a 1-mm separation between them. Their distance from the ground pad is 0.5 mm. The length of the signal trace is 2.0 cm in both cases. The length of the ground trace for Case 2 is 1.5 cm, while for Case 1 an extra length of 2.5 cm is contributed by the portion that runs parallel to the edge of the ground pad until it reaches the ground pin. The characteristic impedance of the differential line formed by the signal and ground trace is 228 Ω and is used as the input source impedance. The signal trace is terminated with a 2-pF capacitor for both cases.

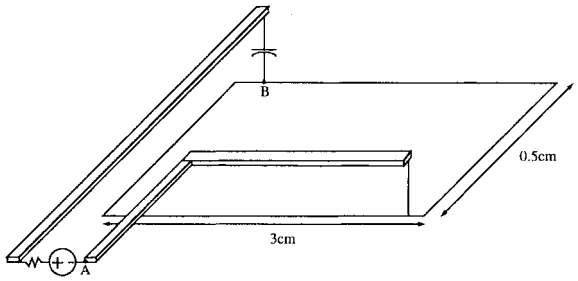

Fig. 12. Geometry of unbalanced package interconnect (Case 1).

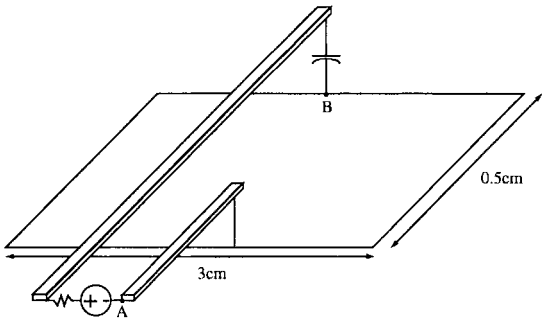

Fig. 13. Geometry of unbalanced package interconnect (Case 2).

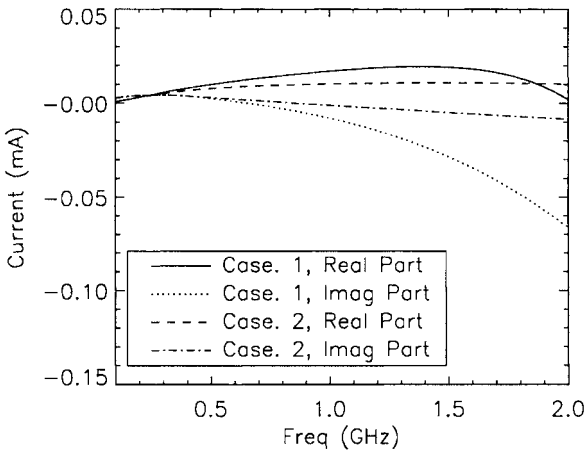

Fig. 14. Common-mode currents.

Fig. 14 compares the common-mode currents at the input of the interconnect for the two cases of ground pin placement. Clearly, Case 2 results in a more *balanced* configuration, and thus the common-mode component of the current is smaller for this case. For the more *unbalanced* case, the magnitude of the common-mode current starts increasing fast for frequencies higher than 1 GHz.

It is often the case that the ground-path inductance is sought for purposes of simultaneous switching noise studies. This quantity can be calculated easily from the results generated by the PEEC. To demonstrate this, consider the geometry of Fig. 13. For the frequency range over which the current through the source and the current through the capacitor are almost equal, the impedance of the return path can be calculated as the ratio of the difference between the voltages at nodes A and B and the current through the source. For

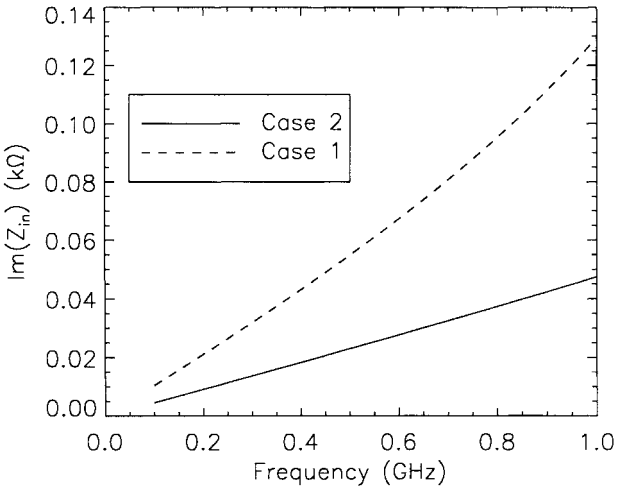

Fig. 15. Imaginary part of effective ground–path impedance.

those frequencies, radiation should be negligible, and the impedance should exhibit an almost inductive behavior. This is confirmed by the curves in Fig. 15 for the imaginary part of the impedance of the ground path for Cases 1 and 2. The slopes of the curves (at the lower frequencies) are the effective inductances for the ground paths. As expected, Case 1 exhibits a higher value of effective ground inductance. Furthermore, it departs faster from the linear behavior due to the greater imbalance in the system.

V. Conclusion

In conclusion, a hybrid electromagnetic modeling and simulation environment has been proposed for the analysis of noise generation and signal-degradation mechanisms in packaged electronic components and systems. Based upon the PEEC formulation, solutions are developed in such a way as to create a hierarchical and robust electromagnetic simulation environment. Of particular importance to this formulation is the ability to effect full-wave electromagnetic solutions in a manner which is compatible with nonlinear circuit simulators such as SPICE. In addition, when the characteristic time of the excitation is such that useful wavelength is much larger than the spatial extent of the system, all retardation effects can be neglected. This type of selective reduction in model complexity of the system is expected to have a positive impact on the computational efficiency of PEEC-based simulators for nonlinear analysis of future high-speed packaged electronics..

References

[1] Y.-S. Tsuei, A. C. Cangellaris, and J. L. Prince, "Rigorous electromagnetic modeling of chip-to-package (first-level) interconnections," *IEEE Trans. Comp. Hybrids, Manufact. Technol.*, vol. 16, pp. 876–883, Dec. 1993.

[2] B. Toland, J. Lin, B. Houhmand, and T. Itoh, "FDTD analysis of an active antenna," *IEEE Microwave Guided Wave Lett.*, vol. 3, pp. 423–425, Nov. 1993.

[3] M. J. Picket-May, A. Taflove, and J. Baron, "FD-TD modeling of digital signal propagation in 3-D circuits with passive and active loads," *IEEE Trans. Microwave Theory Tech.*, vol. 42, pp. 1514–1523, Aug. 1994.

[4] P. Mezzanotte, M. Mongiardo, L. Roselli, R. Sorrentino, and W. Heinrich, "Analysis of packaged microwave integrated circuits by FDTD," *IEEE Trans. Microwave Theory Tech.*, vol. 42, pp. 1796–1801 Sept. 1994.

[5] W. J. R. Hoefer, "Transmission line matrix (TLM) models of electromagnetic fields in space and time," in *Proc. Int. Zurich Symp. EMC*, vol. 11, Zurich, Switzerland, Feb. 1997, pp. 519–522.

[6] B. P. Rynne, "Comments on a stable procedure in calculating the transient scattering by conducting surfaces of arbitrary shape," *IEEE Trans. Antennas Propagat.*, vol. 41, pp. 517–520, Apr. 1993.

[7] A. Sadigh and E. Arvas, "Treating the instabilities in marching-on-in-time methods from a different perspective," *IEEE Trans. Antennas Propagat.*, vol. 41, pp. 1695–1702, Dec. 1993.

[8] A. Ruehli, U. Miekkala, A. Bellen, and H. Heeb, "Stable time domain solutions of EMC problems using PEEC circuit models," in *Proc. Int. Symp. Electromagnetic Compatibility*, Chicago, IL, Aug. 1994, pp. 371–376.

[9] W. Linger and A. Ruehli, "Time domain integration methods for electric field integral equation," *Proc. 1995 Int. Symp. EMC*, Zurich, Switzerland, Mar. 1995, pp. 209–214.

[10] J. Garrett, A. E. Ruehli, and C. R. Paul, "Stability improvement of integral equation models," presented at the *Proc. IEEE Antennas Propagat. Soc. Int. Symp.*, Montreal, Canada, July 1997.

[11] A. E. Ruehli, "Equivalent circuit models for three dimensional multiconductor systems," *IEEE Trans. Microwave Theory Tech.*, vol. MTT-22, pp. 216–221, Mar. 1974.

[12] A. E. Ruehli and H. Heeb, "Circuit models for three-dimensional geometries including dielectrics," *IEEE Trans. Microwave Theory Tech.*, vol. 40, pp. 1507–1516, July 1992.

[13] P. A. Brennan, N. Raver, and A. E. Ruehli, "Three-dimensional inductance computations with partial element equivalent circuits," *IBM J. Res. Develop.*, vol. 23, no. 6, pp. 661–668, Nov. 1979.

[14] A. E. Ruehli, "Inductance calculations in a complex integrated circuit environment," *IBM J. Res. Develop.*, vol. 16, no. 5, pp. 470–481, Sept. 1972.

[15] L. W. Nagel, "SPICE2: A computer program to simulate semiconductor circuits," Electron. Res. Laboratory, Univ. California at Berkeley, Rep. ERL-M520, 1975.

[16] J. L. Drewmiak, T. H. Hubing, and T. P. Van Doren, "Investigation of fundamental mechanisms of common-mode radiation from printed circuit boards with attached cables," in *IEEE Proc. Int. Symp. EMC*, Chicago, IL, Aug. 1994, pp. 110–115.

[17] C. R. Paul, *Introduction to Electromagnetic Compatibility*. New York: Wiley, 1992.

William Pinello received the B.S. degree in electrical engineering from Ohio State University, Columbus, in 1992, the M.S. degree in electrical engineering from the University of Arizona, Tucson, in 1995, and is currently working toward the Ph.D. degree.

He is currently a Graduate Fellow for the Semiconductor Research Corporation, with research interests in the electromagnetic modeling of packaged components and systems for the analysis of noise generation and signal degradation mechanisms.

Andreas C. Cangellaris (M'86), for a biography, see this issue, p. 1867.

Albert Ruehli (M'65–SM'74–F'84) received the Ph.D. degree in electrical engineering from the University of Vermont, Burlington, in 1972.

He has worked at IBM on many different projects, which include mathematical analysis, semiconductor circuits and devices, and as Manager of a VLSI design and CAD group. Since 1972, he has been at the IBM T. J. Watson Research Center, Yorktown Heights, NY, where he is currently a Research Staff Member in the electromagnetic analysis group. He has authored or co-authored over 100 technical papers and has edited *Circuits Analysis, Simulation and Design* (New York: North Holland, 1986, 1987).

Dr. Ruehli is a member of SIAM. He was technical and general chairman of the ICCD International Conference in 1984 and 1985, respectively. He has been a member of the IEEE ADCOM for the IEEE Circuit and System Society, and an associate editor for the IEEE Transactions on Computer-Aided Design. He has spoken at numerous conferences and universities, and has organized many sessions.